Engineering Failure Analysis 186 (2026) 110563

Contents lists available at ScienceDirect

Engineering Failure Analysis

journal homepage: www.elsevier.com/locate/engfailanal

Failure mechanisms and structural response of CIPP-Rehabilitated concrete pipes under external loads

Jing Liu [a,1], Jingguo Cao [b,1], Chang Ma [a], Wenlin Jing [c], Kangfu Sun [b,d,*], Tingting Yang [e,**]

[a] College of Marine and Environmental Sciences, Tianjin University of Science & Technology, 300457 Tianjin, China
[b] College of Chemical Engineering and Materials Science, Tianjin University of Science & Technology, 300457 Tianjin, China
[c] China Construction Infrastructure Co.Ltd., Beijing 100044, China
[d] Ningbo Water Meter (Group) Co., Ltd., Ningbo 315000, China
[e] Tianjin North China Geological Exploration Bureau, Tianjin 300170, China

ARTICLE INFO

Keywords:
Reinforced concrete pipe(RCP)
Cured-in-place pipe(CIPP) lining
Three-edge bearing test (TEBT)
Failure mechanism
Stiffness superposition

ABSTRACT

Cured-in-place pipe (CIPP) lining is widely used to restore deteriorated concrete drainage pipes; however, the failure evolution and composite load-bearing behavior of rehabilitated pipelines under external loads remain poorly quantified. This study conducted full-scale three-edge bearing tests (TEBT) on intact, corroded, and rehabilitated reinforced concrete pipes (RCPs) to clarify how corrosion defects and liner stiffness jointly influence structural performance. Artificial corrosion was introduced via controlled high-pressure water milling, and two rehabilitation configurations—5 mm semi-structural and 12 mm structural liners—were applied. Circumferential strain responses and crack development were continuously monitored using strain gauges and distributed optical-fiber sensing. Results show that the 12 mm structural liner increased the cracking and ultimate loads by 10–26 %, redistributed strain, and shifted the failure mode from brittle concrete crushing to a ductile composite response with a secondary yield plateau. In contrast, the 5 mm semi-structural liner decreased the ultimate load by up to 17 % due to circumferential stiffness mismatch combined with interface debonding, which prevented effective composite action. Mechanistic analysis reveals that stiffness superposition and neutral-axis migration jointly govern the enhanced bending resistance and ductility of the rehabilitated system. These findings elucidate the external load failure mechanisms of CIPP-reinforced RCPs and provide performance-based guidance for selecting liner stiffness and designing structural rehabilitation strategies for buried pipelines.

1. Introduction

Concrete drainage pipes progressively deteriorate under long-term exposure to aggressive environments, external loading, and

* Corresponding author at: No.9, Thirteenth Street, Binhai New Area Economic and Technological Development Zone, Tianjin, Tianjin University of Science & Technology, Tianjin 300457, China.
** Corresponding author at: Tianjin North China Geological Exploration Bureau, No. 67 Guangrui West Road, Hedong District, Tianjin 300170, China.
E-mail addresses: skf@tust.edu.cn (K. Sun), yangtt210@126.com (T. Yang).
[1] These authors Contributed equally: Jing Liu, Jingguo Cao.

https://doi.org/10.1016/j.engfailanal.2026.110563
Received 1 November 2025; Received in revised form 15 December 2025; Accepted 8 January 2026
Available online 9 January 2026
1350-6307/

structural defects, resulting in stiffness degradation, crack propagation, and reduced load-bearing capacity [1,2]. Cured-in-place pipe (CIPP) lining has become an important trenchless rehabilitation method due to its installation efficiency and broad applicability [3–5]. Nevertheless, the composite interaction between CIPP liners and concrete pipes under external loads, particularly their failure evolution and structural contribution, remains insufficiently quantified [6,7].

Previous studies have demonstrated that internal liners can substantially enhance the structural performance of deteriorated concrete pipes. Law and Moore [8], Smith *et al.* [9], and Riahi *et al.* [10] conducted load-bearing tests on pipes lined with HDPE, steel–grout–HDPE, and epoxy, respectively, showing that liners effectively increase circumferential stiffness and load capacity, with epoxy liners of 3–12 mm achieving improvements of 6–40 %. Different lining materials (e.g., epoxy, CFRP, and other composite systems) have been shown to strengthen cracked sections, delay damage progression, and improve residual capacity [11,12]. Wang *et al.* [13] evaluated PE–CIPP composite structures under external loads and found that CIPP liners increased pipe stiffness and load capacity by 200–500 %. He *et al.* [14] assessed the role of residual prestress and observed that rehabilitated pipes tended to fail through longitudinal cracking and interfacial delamination.

Extensive studies have investigated the load-bearing behavior of deteriorated concrete pipes reinforced with CIPP liners. Model- and full-scale experiments (Shou and Chen [15]; Fang *et al.* [16]; Li and Fang [17]; Hsu and Shou [18]; Takahashi [19]; Gumble *et al.* [20]) consistently show that integrating a CIPP liner with a rigid host pipe increases circumferential stiffness and reduces vertical deformation under radial loading. Yang *et al.* [21] identified surface traffic load as the dominant factor governing composite pipe performance, with internal fluid pressure having negligible effect, while Fang *et al.* [22] showed that misaligned bell-and-spigot joints are most critical under traffic loading and that increasing liner thickness or flexural modulus enhances post-rehabilitation strength. Yang *et al.* [23] showed that joint-adjacent voids intensify stress concentrations in CIPP liners, while Yan *et al.* [24] found that crown cracking reduces the cracking load and that increased liner thickness partially restores capacity.

While CIPP rehabilitation is known to enhance structural performance, the mechanics of the flexible–rigid composite system remain poorly understood because key processes—neutral-axis migration, stiffness interaction, and stress redistribution under external loading—have not been quantitatively characterized.

In addition, existing evaluations under different damage levels are often qualitative or case-specific, limiting their general applicability. Consequently, several critical gaps remain. First, prior work has focused primarily on deformation of the original host pipe, with insufficient attention to the coordinated mechanical behavior and failure modes of the CIPP–concrete composite structure. Second, the mechanical distinction between semi-structural and fully structural CIPP liners has not been systematically quantified. Third, the influence of liner thickness and modulus is often empirically described rather than mechanistically established. Fourth, compatibility between CIPP liners and host pipes with varying corrosion deterioration remains unclear, restricting their application in structural design.

To address these gaps, this study conducted full-scale three-edge bearing tests (TEBT) on intact and corroded reinforced concrete pipes rehabilitated with CIPP liners of two stiffness levels (semi-structural and structural). The experiments quantified the effects of corrosion, liner stiffness, and interface behavior on the external load capacity and failure evolution of CIPP–concrete composite systems. Circumferential strains, crack development, and composite action were analyzed to elucidate the underlying strengthening mechanisms and provide a rational basis for structural rehabilitation design.

2. Materials and Methods

The experimental program consisted of four comparative test groups: (1) plain reinforced concrete pipe (RCP); (2) corroded RCP; (3) RCP–CIPP composite pipe; and (4) corroded RCP–CIPP composite pipe. The detailed configuration of each group is presented in Table 1.

2.1. Test materials and Equipment

The tested specimens were Class II reinforced concrete pipes (RCPs) with dimensions of 500 mm × 55 mm × 2000 mm and 800 mm × 80 mm × 2500 mm, both equipped with B-type bell-and-spigot joints and flexible connections. Corroded and intact pipes shared identical reinforcement ratios; the steel cages were fabricated from 5 mm plain steel bars and welded into circular forms. For the corroded specimens, the inner crown of each pipe was milled using a high-pressure water jet until the reinforcement was exposed, creating a defect measuring 280 mm × 60 mm × 2500 mm, as illustrated in Fig. 1.

This artificial defect reflects the crown deterioration frequently documented in CCTV inspection records and field investigations

Table 1
Experimental Loading Conditions.

Group	Specimen	Pipe			Other processing		Quantity
		Nominal diameter(mm)	length(mm)	Wall thickness(mm)	Corrosion defect	CIPP liner	
1	RCP 500	500	2140	55	×	×	3
2	RCP800-Corr0	800	2500	80	×	×	3
3	RCP800-Corr60	800	2500	80	√	×	3
4	RCP500-CIPP5	/	2140	55 + 5	×	√	3
5	RCP800-Corr0-CIPP12	/	2500	80 + 12	×	√	3
6	RCP800-Corr60-CIPP12	/	2500	80 + 12	√	√	3

[25–27], where acidic effluents, biogenic sulfuric corrosion, and abrasive flows typically form axially elongated corrosion bands of moderate to severe depth. For DN800 pipes, the adopted geometry corresponds to approximately 75 % inner-wall thickness loss, representing a severe but non-perforating deterioration level consistent with practical observations.

The crown was selected because it is the critical location governing flexural failure under external loads, and previous studies have shown that crown defects accelerate crack initiation and markedly reduce load-bearing capacity [28,29]. This corrosion configuration therefore provides a representative damage scenario for evaluating the strengthening contribution of CIPP liners.

Based on the semi-structural and structural rehabilitation design specifications in T/CECS 59 *Technical Code for In-situ Cured Pipe Rehabilitation for Water Supply and Drainage Pipelines*, the calculated liner thicknesses were 4.95 mm and 11.8 mm, which were rounded to 5 mm and 12 mm, respectively.

The CIPP liners used in this study consisted of fiberglass fabric impregnated with an unsaturated polyester resin. A medium-sized UV-curing system equipped with a 4 × 1000 W high-pressure mercury lamp was employed to rehabilitate 15 m-long DN800 concrete pipes, simulating the in-situ repair process of underground drainage pipelines. The preparation and curing procedures are illustrated in Fig. 2.

(a) A protective membrane was fixed at both ends to cover one-third of the pipe circumference, preventing liner abrasion.
(b) The liner was pulled into the concrete pipe at a rate of 5 m/min using a winch-driven rope.
(c) Safety collars were installed at both ends, and exposed sections were wrapped as required.
(d) After the blower reached stable operation, the liner was inflated and maintained under pressure, while the UV lamp guide rope replaced the pull rope.
(e) The lamp carriage was inserted, end plates sealed, and internal pressure increased to 250 mbar to ensure full contact with the host pipe wall, monitored by an internal camera.
(f) The UV lamp chain was then activated and advanced at a constant speed of 0.3 m/min for curing, after which pressure was gradually released to atmospheric level.

After rehabilitation, the CIPP liner specimens exhibited uniform wall thickness with no visible distortion, surface scratches, voids, or depressions. Mechanical testing was conducted using a computer-controlled universal testing machine. Tensile specimens (200 mm × 20 mm × 12 mm) and flexural specimens (192 mm × 20 mm × 12 mm) were both tested at a loading rate of 2 mm/min. The resulting mechanical properties, summarized in Table 2, satisfied the requirements for subsequent external pressure tests.

The layout of the test setup and instrumentation is shown in Fig. 3. Strain gauges were mounted at the crown, invert, and springline positions on both the inner and outer walls of the RCP and RCP–CIPP composite pipes (with the crown defined as 0°, proceeding clockwise to 90°, 135°, 180°, and 270°). An eight-channel strain recorder continuously monitored stress–strain variations at different wall positions during loading (Fig. 4a). In addition, distributed fiber-optic sensors were installed circumferentially on the inner wall of the RCP and RCP–CIPP composite pipes, at a distance of 1 m from the joint edge, to measure circumferential strain distributions during the loading process (Fig. 4b).

2.2. Test Methods

The tested pipe specimens were Class II reinforced concrete pipes with a strength grade of C45. The crack load and ultimate load tests were performed in accordance with *Concrete and Reinforced Concrete Drainage Pipes* (GB/T 11836–2023) and *Test Methods for Concrete and Reinforced Concrete Drainage Pipes* (GB/T 16752–2017). The detailed test indicators and parameters are summarized in Table 3.

The external load tests were carried out using a reinforced concrete pipe compression testing machine. Loads of 102.72 kN and 202.5 kN were applied to DN500 (straight section length 2140 mm) and DN800 (straight section length 2500 mm) pipes, respectively, based on the product of the straight section length and the specified test criteria. The loading rate was maintained at 30.0 kN/(m·min). Each specimen was first loaded to 80 % of the ultimate load and held for 1 min for observation. If no visible cracking occurred, the load was increased in 10 % increments (90 %, 100 %), each stage held for 1 min. At 100 % of the ultimate load, the load was sustained for 3 min. If the specimen remained intact, the load was subsequently increased in 5 % increments (105 %,110 %, …), with each stage

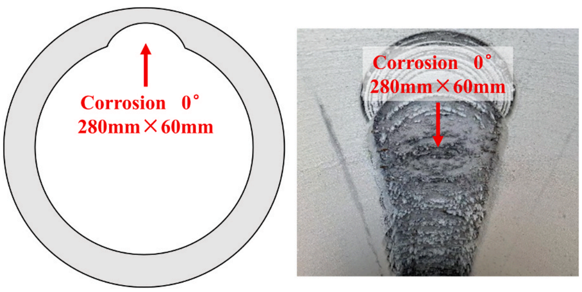

Fig. 1. Corrosion of RCP Pipe.

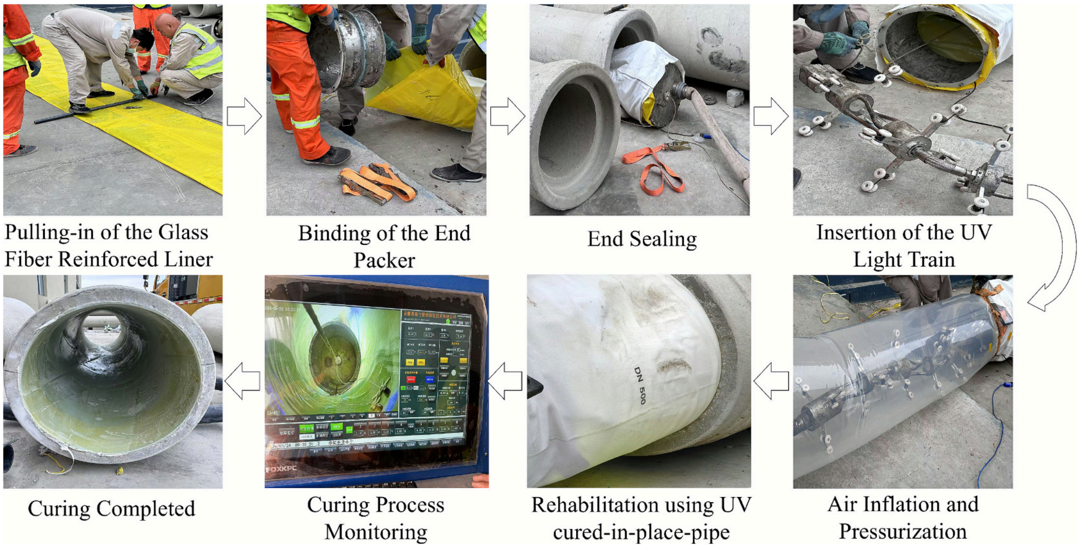

Fig. 2. CIPP Lining Preparation Process.

Table 2
Mechanical Properties of the Rehabilitated Liner.

Property	Requirement	Measured value	Pipe diameter	Test method
Average wall thickness (mm)	≥5	5	DN500	Determination of Dimensions of Plastic Components for Plastic Pipeline Systems GB/T 8806
	≥12	12.67	DN800	
Tensile strength (MPa)	≥80	165	DN500	Determination of Tensile Properties of Plastics—Part 4: Test Conditions for Isotropic and Orthotropic Fiber-Reinforced Composites GB/T 1040.4
		147.64	DN800	
flexural strength (MPa)	≥125	207	DN500	Test Method for Flexural Properties of Fiber-Reinforced Plastics GB/T 1449
		158.88	DN800	
flexural modulus(MPa)	≥8000	10,413	DN500	
		14,360	DN800	
Brinell hardness on polished surfaces (HBa)	≥45	64	DN500	Test Method for Barcol Hardness of Reinforced Plastics GB/T 3854
		54	DN800	
Backlight surface Barcol hardness (HBa)		62	DN500	
		55	DN800	
Ring stiffness (kN/m^2)	/	0.82	DN500	Determination of Ring Stiffness of Thermoplastic Pipes GB/T 9647
		4.98	DN800	

maintained for 3 min, until structural failure occurred.

2.3. Difference between TEB test and in-situ buried pipe stress conditions

The three-edge bearing (TEB) test adopted in this study follows ASTM C497 and is a standardized method for evaluating the circumferential flexural capacity of reinforced concrete pipes. Its primary significance lies in imposing simplified yet well-defined boundary conditions that isolate bending as the dominant structural response under external loading. By applying a vertical line load at the crown with rigid supports at the invert, the TEB configuration establishes a clear load path and a stable, repeatable bending-moment distribution at the crown, invert, and springlines, providing a consistent basis for assessing the structural contribution of CIPP liners.

In contrast, the mechanical behavior of buried pipelines is strongly influenced by soil–structure interaction effects, including lateral confinement, soil arching, and backfill variability, resulting in complex and scattered stress states. While buried conditions more closely resemble in-service environments, this complexity can obscure the intrinsic strengthening effect of the liner, making it difficult to distinguish liner-induced improvements from soil confinement effects.

From a structural assessment perspective, a key advantage of the TEB test is that it provides an intentionally unfavorable, soil-free boundary condition, under which the liner–host pipe system is directly challenged in bending without lateral support. Strengthening effects observed under such conditions may therefore be regarded as a conservative, lower-bound evaluation of liner performance.

Moreover, in several practical situations—including shallow cover installations, traffic-induced loading, and pipelines affected by

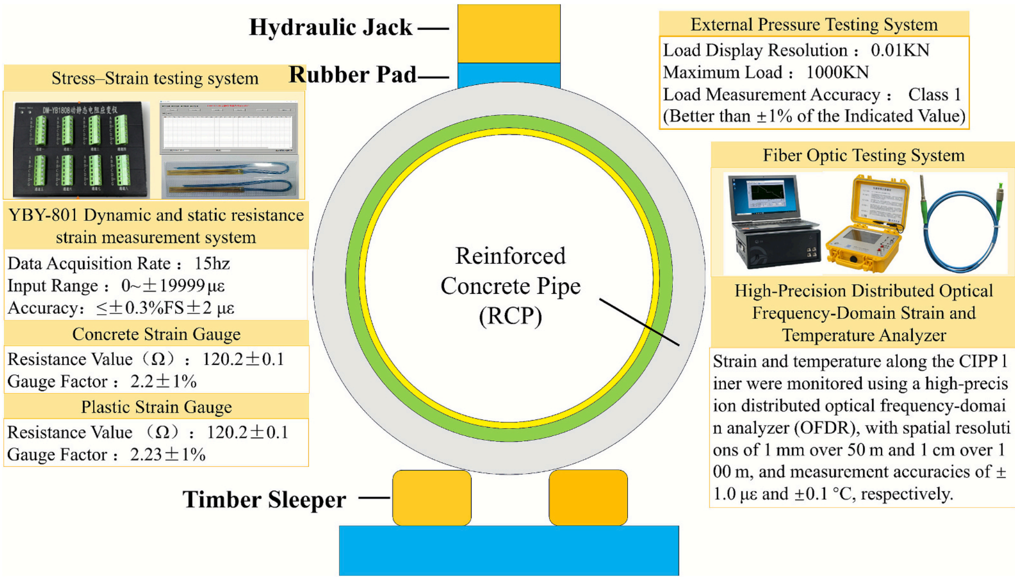

Fig. 3. Schematic Diagram of External Pressure Test Apparatus.

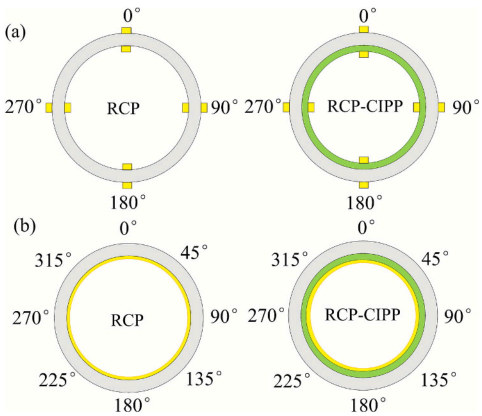

Fig. 4. Strain gauge arrangement:(a) Strain gauge layout, and (b) Fiber optic cable layout diagram.

Table 3
Specifications of Reinforced Concrete Pipes and External Load Test Criteria.

Nominal diameter (mm)	Effective length (mm)	Wall thickness (mm)	Crack load kN/m	Destructive load kN/m	Internal water pressure (MPa)
500	≥1000	≥55	32	48	0.1
800		≥80	54	81	

crown corrosion or localized stiffness degradation—structural response is often governed by bending behavior similar to that captured by the TEB configuration. Accordingly, although the TEB test does not reproduce the full in-situ stress environment, it effectively captures a critical and practically relevant failure mechanism for rigid and CIPP-rehabilitated pipes under external loading.

3. Results and discussion

The results of the external load tests for the RCP and RCP–CIPP composite pipes are summarized in Table 4.
*The increment of load-bearing capacity is defined as:

$$\Delta R = \frac{R_{\text{after repair}} - R_{\text{before repair}}}{R_{\text{before repair}}}$$

Table 4
Comparison of External Load Test Results of Pipes.

Specimen	Crack load (kN)	Average crack load (kN)	Ultimate load (kN)	Average ultimate load (kN)	Increase in crack load capacity* (%)	Increase in ultimate load capacity* (%)
RCP 500	140.00	140.08	210.33	210.67	/	/
	140.24		220.00			
	140.00		202.02			
RCP500 −CIPP5	120.15	138.34	189.22	174.86	−1.24 %	−17.00 %
	143.99		160.63			
	150.88		174.73			
RCP800-Corr0	217.40	186.80	317.00	265.00	/	/
	163.00		237.00			
	180.00		241.00			
RCP800-Corr0-CIPP12	234.01	234.77	300.04	293.55	25.68 %	10.77 %
	260.30		280.05			
	210.00		300.56			
RCP800-Corr60	169.74	146.58	235.22	225.07	/	/
	150.00		210.00			
	120.00		230.00			
RCP800-Corr60-CIPP12	170.24	176.69	278.00	265.80	20.54 %	18.10 %
	180.06		261.02			
	179.77		258.38			

where $R_{\text{before repair}}$ and $R_{\text{after repair}}$ represent the load-bearing capacities prior to and following the repair, respectively.

Following rehabilitation of the DN500 pipeline with a semi-structural CIPP liner, the cracking load decreased by 1.24 %, and the ultimate load dropped by 17.00 %. This reduction was mainly caused by the annular gap between the liner and the host pipe wall, which impeded effective load transfer, weakened the composite action, and produced stress concentrations at defect locations, thereby accelerating structural failure. In addition, possible construction-related deficiencies—such as nonuniform liner thickness, incomplete curing, or local weak spots—may have further reduced the overall stiffness and load-bearing capacity. These issues require further verification through detailed inspection of lining parameters, including thickness uniformity and conformity to the design values.

Wang *et al.* [30] reported that, in external hydrostatic buckling tests on DN600 CIPP-lined pipes, a 5 % increase in ovality resulted in a 10.62 % reduction in the critical buckling pressure, demonstrating the strong sensitivity of liner performance to initial geometric imperfections. This observation is consistent with the results of the present study, which likewise indicate that semi-structural CIPP linings are not suitable for pipelines with pronounced pre-existing defects.

The cracking and ultimate loads of the intact pipes (RCP800-Corr0) were markedly higher than those of the corroded pipes (RCP800-Corr60), confirming that corrosion substantially reduces the load-bearing capacity. Once the concrete in the corroded zone failed, the applied load was transferred mainly to the remaining section and the exposed reinforcement. In intact pipes, the reinforcement works compositely with the surrounding concrete through bond stresses; by contrast, in corroded pipes, the reinforcement is more directly loaded and therefore more prone to yielding. Moreover, stress concentrations at the defect edges promote crack propagation and further accelerate strength degradation.

The repair performance of the DN800 pipes was evaluated by comparing intact lined pipes (RCP800-Corr0-CIPP12) and corroded lined pipes (RCP800-Corr60-CIPP12). The repaired corroded pipe showed a greater increase in ultimate load (18.10 %) than the repaired intact pipe (10.77 %), indicating that structural CIPP lining is more effective for deteriorated pipelines. The capacity loss of the corroded pipe was mainly due to section reduction, reinforcement corrosion, and local spalling. The structural liner filled damaged regions and redistributed part of the external load, leading to a more substantial recovery in strength.

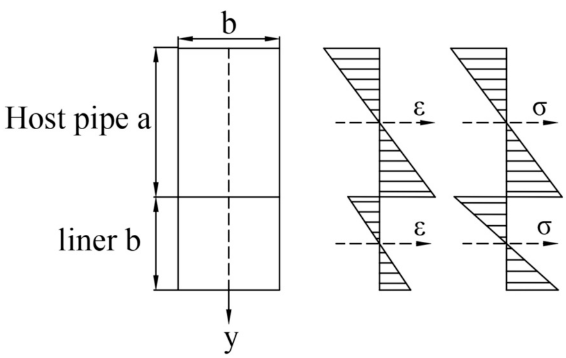

Fig. 5. Composite Beam Force Model.

3.1. Mechanistic differences in Load-Bearing performance between Semi-Structural and structural CIPP Repairs

3.1.1. Load-Bearing capacity calculation method based on the composite beam model

The composite beam is a commonly used structural form in building and bridge engineering, consisting of steel members integrated with concrete slabs to enhance overall stiffness and load-bearing capacity [31]. In this study, composite beam theory was employed to analyze the mechanical behavior of the concrete pipe–CIPP lining system. The analysis neglects secondary stress effects and considers only the structural response under combined axial force and bending moment. A schematic diagram of the analytical model is shown in Fig. 5.

(1) Basic Assumptions

A 1 m-long pipe segment was idealized as a plane beam satisfying the plane-section assumption. The concrete compression zone was represented by a rectangular stress block, while the tensile strength of concrete was neglected. Both the steel reinforcement and the CIPP liner were taken to reach their design strengths, f_y and f_f. Interfacial slip was omitted to derive a closed-form expression for bending resistance.

It should be noted that the UV-cured CIPP liner is not chemically bonded to the concrete; the interface is frictional rather than adhesive. The no-slip approximation does not imply perfect bonding but reasonably reflects the deformation compatibility observed in the TEBT for the 12 mm structural liner, which provides sufficient circumferential stiffness to mobilize composite action. In contrast, thinner or semi-structural liners may exhibit limited shear transfer and local separation, diminishing their composite efficiency. This limitation suggests that future analytical models should incorporate frictional interfaces or shear-transfer laws for improved accuracy.

(2) Geometry and Strain Coordination

Strain at an arbitrary height y under the plane-section assumption:

$$\varepsilon(y) = \varepsilon_{cu}\frac{y}{x} \tag{1}$$

Tensile strain of the outermost fibers of the CIPP lining:

$$\varepsilon_f = \varepsilon_{fu}\frac{h-x}{x} \tag{2}$$

Tensile strain of the reinforcement:

$$\varepsilon_s = \varepsilon_{cu}\frac{h_0-x}{x} \tag{3}$$

(3) Internal Force Equilibrium

Compression zone:

$$C = 0.8bxf \tag{4}$$

Tension zone:

$$T = A_sE_c\varepsilon_s + bt_fE_f\varepsilon_f \tag{5}$$

Applied strain compatibility:

$$T = A_sE_c\varepsilon_{cu}\frac{h_0-x}{x} + bt_fE_f\varepsilon_{fu}\frac{h-x}{x} \tag{6}$$

By setting $C = T$ and rearranging, a quadratic equation in terms of x is obtained.

$$0.8bf_cx^2 - \varepsilon_{cu}\left[A_sE_c(h_0-x) + bt_fE_f(h-x)\right] = 0 \tag{7}$$

(4) Ultimate Bending Moment M_u

Take moments about the resultant force of the compression zone:

$$M_u = A_s\sigma_s(h_0 - 0.4x) + bt_f\sigma_f(h - 0.4x - 0.5t_f) \tag{8}$$

Strain Compatibility Model:$\sigma_s = E_c\varepsilon_s \leq fy, \sigma f = E_f\,\varepsilon_f \leq f_f$; .
Plastic model:$\sigma_s = f_y, \sigma_f = f_f$; .

(5) Three-edge bearing load limit value:

$$P_u = \frac{4M_u}{L} \tag{9}$$

In the formula: ε_{cu}—ultimate compressive strain of concrete; x—neutral axis depth; ε_{fu}—ultimate tensile strain of CIPP; h—total pipe wall thickness; t_f—CIPP layer thickness; h_0—effective depth of reinforcement; b—effective width for calculation(=1000 mm); f_c—design compressive strength of concrete; A_s—cross-sectional area of tension reinforcement; E_c—Elastic modulus of concrete; E_f—Elastic modulus of CIPP;L—Center-to-center distance of supports.

3.1.2. Mechanistic study of the adverse effects of Semi-Structural repair on compressive strength of rigid pipes

As shown in Fig. 6, installing a 5 mm CIPP liner reduced the ultimate load of the DN500 RCP by 17 %. This adverse effect resulted from a stiffness–strength mismatch: the elastic modulus of the CIPP is only about 30 % that of concrete, leading to a marked reduction in flexural stiffness. The 0.5–2 mm annular gap created a "cavity hinge", disrupting composite action and generating stress concentrations 1.5–2 times higher than in adjacent regions, thereby accelerating concrete crushing. Nonuniform liner thickness (±1 mm) and areas of incomplete curing (below 80 %) further decreased the effective section by roughly 15 %, aggravating the loss of stiffness and bearing capacity.

Regarding strain distribution, the peak tensile strain on the pipe's outer wall decreased from 9000 με to 1500 με (decreased by 75 %), while part of the tensile stress was transferred to the liner, increasing CIPP strain to over 3000 με without failure. This stress redistribution produced a steep compressive strain gradient, forming a negative redistribution mechanism characterized by a stable tensile zone and premature compressive failure. Overall, the combined effects of insufficient liner stiffness, annular gaps, and local quality deficiencies reduced compressive strength; these effects can be mitigated by increasing liner thickness and ensuring uniformity and complete curing during installation.

3.1.3. Mechanistic study of the Beneficial effects of structural repair on compressive strength of rigid pipes

The circumferential strain distribution along the inner wall and the load–strain responses of the DN800 RCP and composite pipes are shown in Figs. 7 and 8. After structural CIPP rehabilitation, the cracking load increased from 187 kN to 234 kN (increased by 25 %), while the circumferential tensile strain at the crown (0°) decreased from 9000 με to 1500 με (decreased by 83 %). The ultimate load increased from 265 kN to 300 kN (increased by 13 %), with the failure region extending over more than 10 % of the pipe circumference, and the circumferential compressive strain decreasing from 3000 με to 1000 με (decreased by 67 %).

The 12 mm uniform CIPP liner formed a high-modulus circumferential tensile layer along the inner wall, effectively sharing tensile stress during the elastic stage and reducing concrete strain. The neutral axis shifted inward, alleviating the compressive strain gradient and establishing a cooperative load-bearing mechanism characterized by a "tensile zone reinforced by steel—compressive zone stabilized." The CIPP sustained high tensile strain without rupture, providing a ductility-like plateau. Consequently, structural rehabilitation improved both the compressive strength and deformation capacity of the rigid pipes through a mechanism described as "circumferential stiffness superposition—strain redistribution—retention of compressive safety margin."

3.2. Quantitative influence of initial corrosion level on load enhancement by structural CIPP repair

The circumferential strain distribution along the inner wall and the load–strain behavior at different locations of the corroded and repaired DN800 pipes are shown in Fig. 9 and Fig. 10. Corrosion at the crown reduced the load-bearing capacity of the DN800 RCP to 230 kN, accompanied by a peak strain of 10,000 με. After rehabilitation with a 12 mm uniform CIPP liner, the capacity recovered to 258 kN (+12 %), while the peak strain decreased sharply to 2500 με (−75 %), equivalent to an average gain of 2.3 kN and a strain reduction of 625 με per millimeter of liner thickness. Following corrosion-induced wall thinning, the ultimate moment provided by the

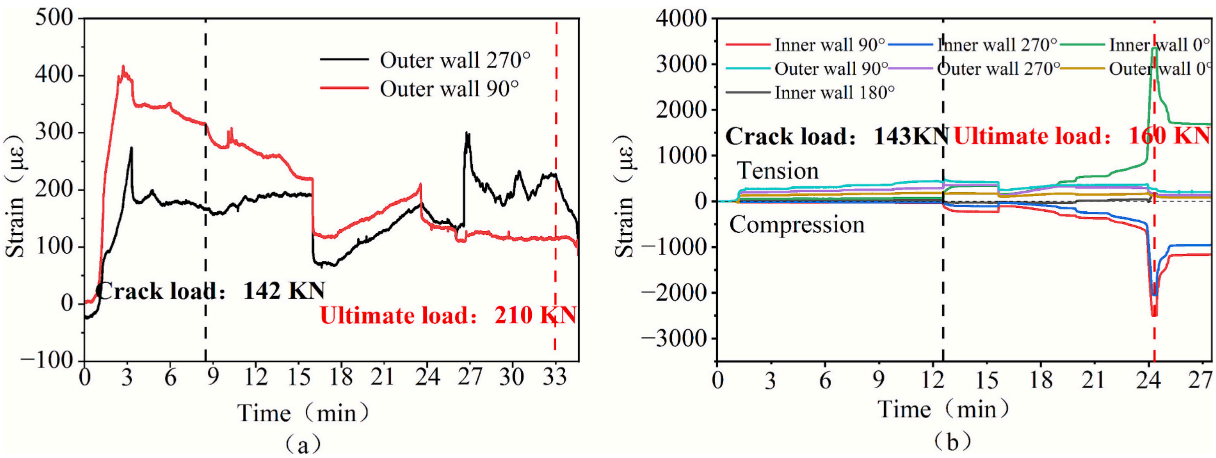

Fig. 6. Pipe wall strains of DN500 RCP before and after repair: (a) RCP500, and (b) RCP500-CIPP5.

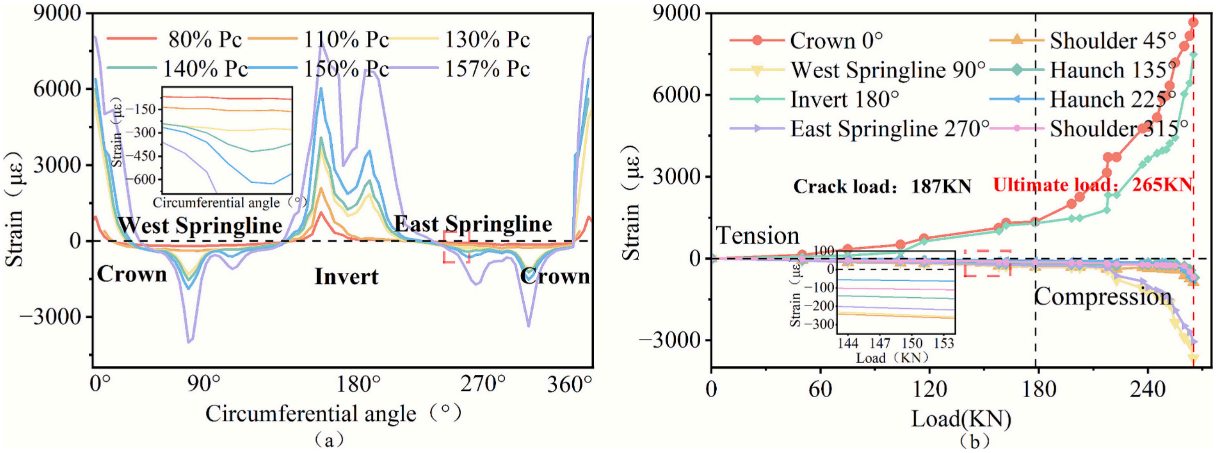

Fig. 7. Inner wall response of DN800 RCP: (a) circumferential strain, and (b) load–strain relationship.

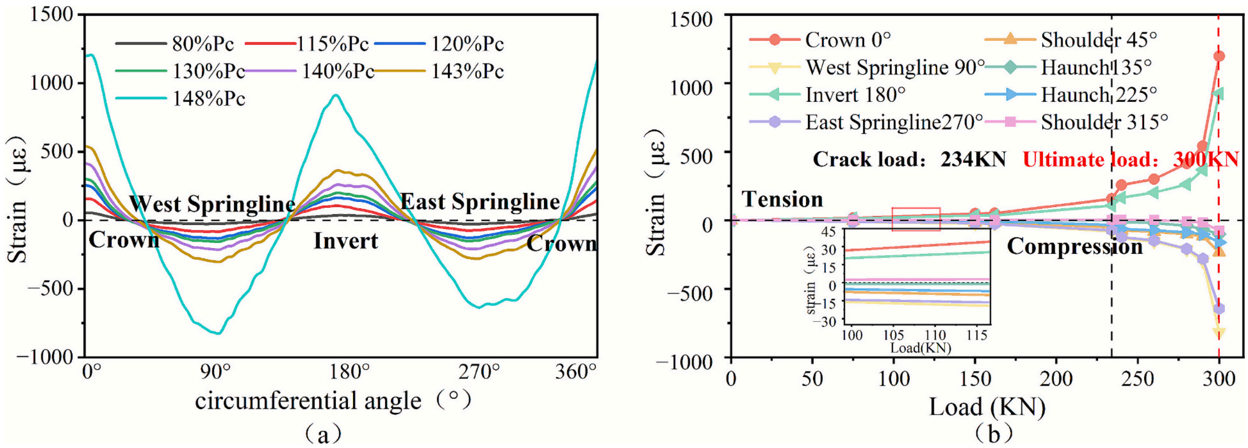

Fig. 8. Inner wall response of DN800 RCP-CIPP composite pipe: (a) circumferential strain, and (b) load–strain relationship.

concrete compression zone was substantially reduced. The tensile force developed in the liner, together with the remaining concrete compression, formed a new internal moment couple that quantitatively compensated for the loss caused by corrosion, resulting in a bending capacity exceeding that of the original corroded pipe. These results confirm the positive load-restoration mechanism of

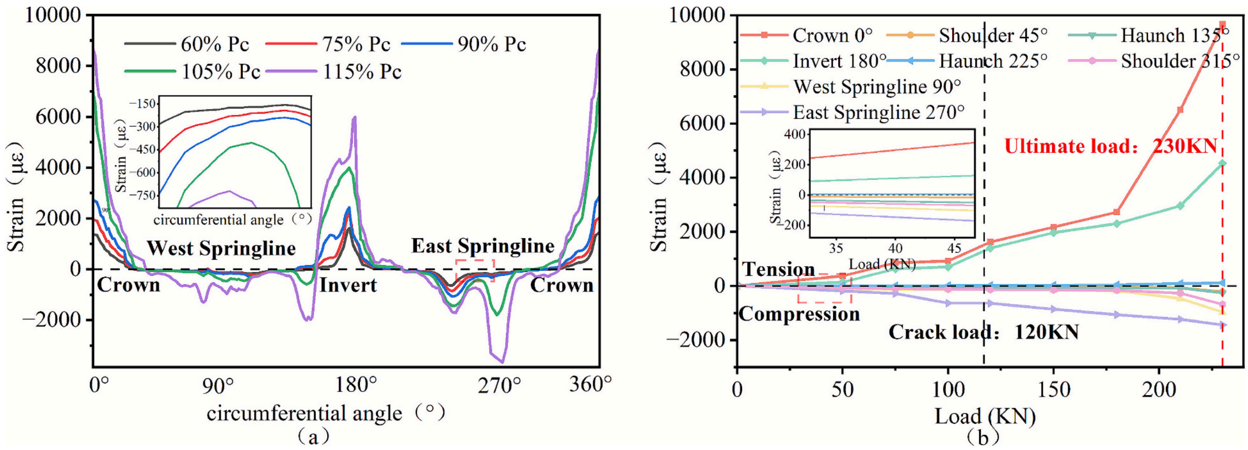

Fig. 9. Inner wall response of corroded DN800 RCP: (a) circumferential strain, and (b) load–strain relationship.

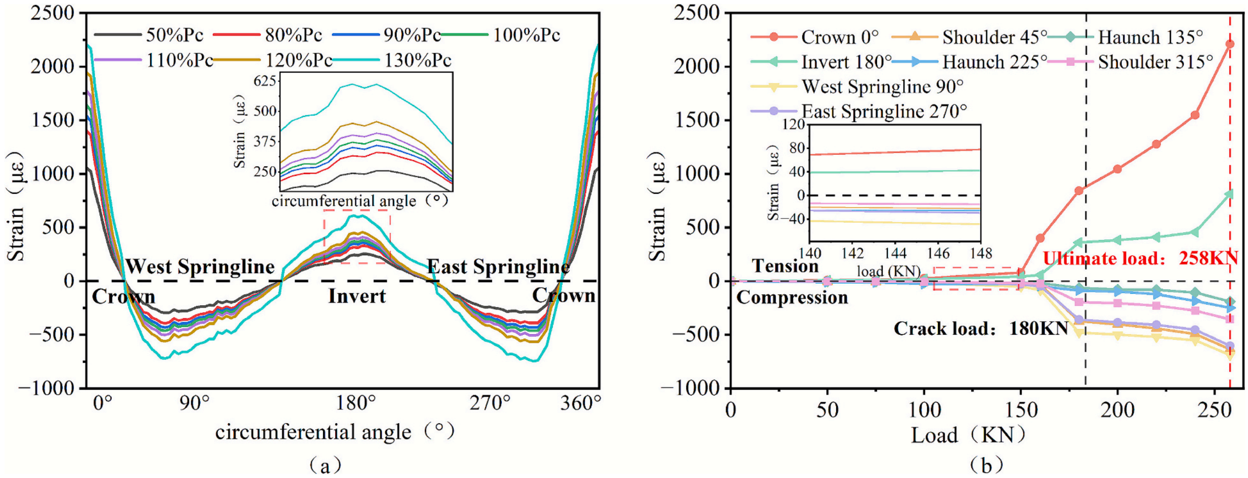

Fig. 10. Inner wall response of corroded DN800 reinforced concrete–CIPP composite pipe: (a) circumferential strain, and (b) load–strain relationship.

structural CIPP repair and provide a quantitative reference for corrosion–thickness matching in rehabilitation design.

3.3. Mechanistic Insights into CIPP-Induced Asynchrony between crack resistance and ultimate load in pipelines

As shown in Fig. 11, the load–strain responses of the bare RCP and the CIPP-composite pipes differed markedly. During the elastic stage, both exhibited nearly linear growth, but the composite pipe showed more coordinated behavior due to the tensile contribution of the liner. In the plastic stage, the strain in the bare pipe increased sharply, leading to rapid instability, whereas the composite pipe displayed a slower strain rate as the liner restrained crack propagation. At failure, the bare pipe underwent brittle collapse with a steep curve drop, while the composite pipe exhibited a plateau or gradual decline, maintaining load-bearing capacity and demonstrating improved ductility.

The CIPP liner modified the structural response through a three-stage mechanism—“strain suppression in the elastic stage, slope reduction in the plastic stage, and plateau maintenance in the failure stage”—transforming the brittle failure of the bare pipe into a controlled ductile mode. This confirms the asynchronous yet synergistic enhancement of crack resistance and ultimate load provided by the liner.

As shown in Fig. 12, the CIPP liner precisely regulated the mechanical behavior of both corroded and intact pipes through an asynchronous progressive mechanism of “elastic-stage crack resistance—plastic-stage gradual failure—ductile plateau at failure.” During the elastic stage, the liner immediately shared tensile stress, suppressing crack initiation. In the plastic stage, it continued to elongate beyond 3000 με without rupture, transforming crack propagation from a rapid surge into a gradual process. At failure, the liner provided residual tensile capacity, converting the load–strain curve from a steep drop to a plateau and achieving a brittle-to-ductile transition. This mechanism confirms the liner’s ability to synchronously enhance crack resistance and ultimate load capacity.

As shown in Fig. 13, the 0°, 90°, 180°, and 270° positions correspond to strain-sensitive regions where circumferential strain rises or

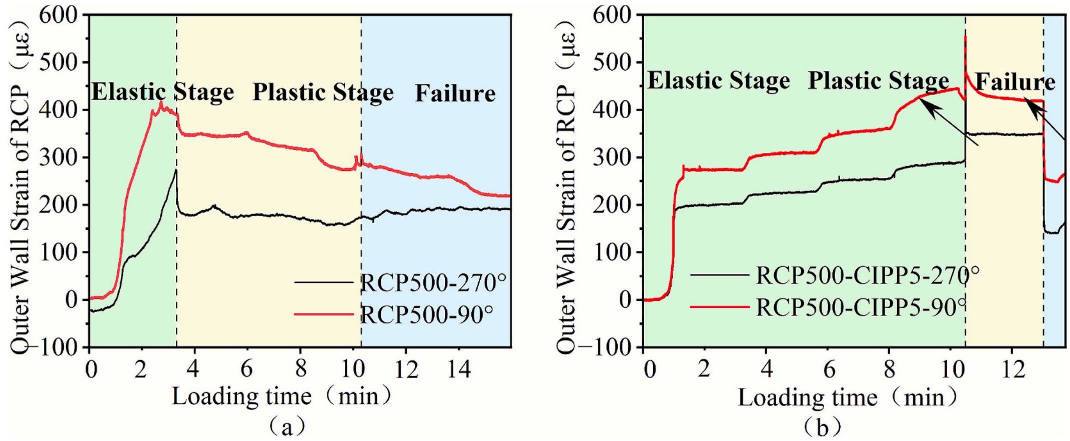

Fig. 11. Time–strain curves of DN500 single and composite pipes:(a)RCP, and (b)RCP-CIPP.

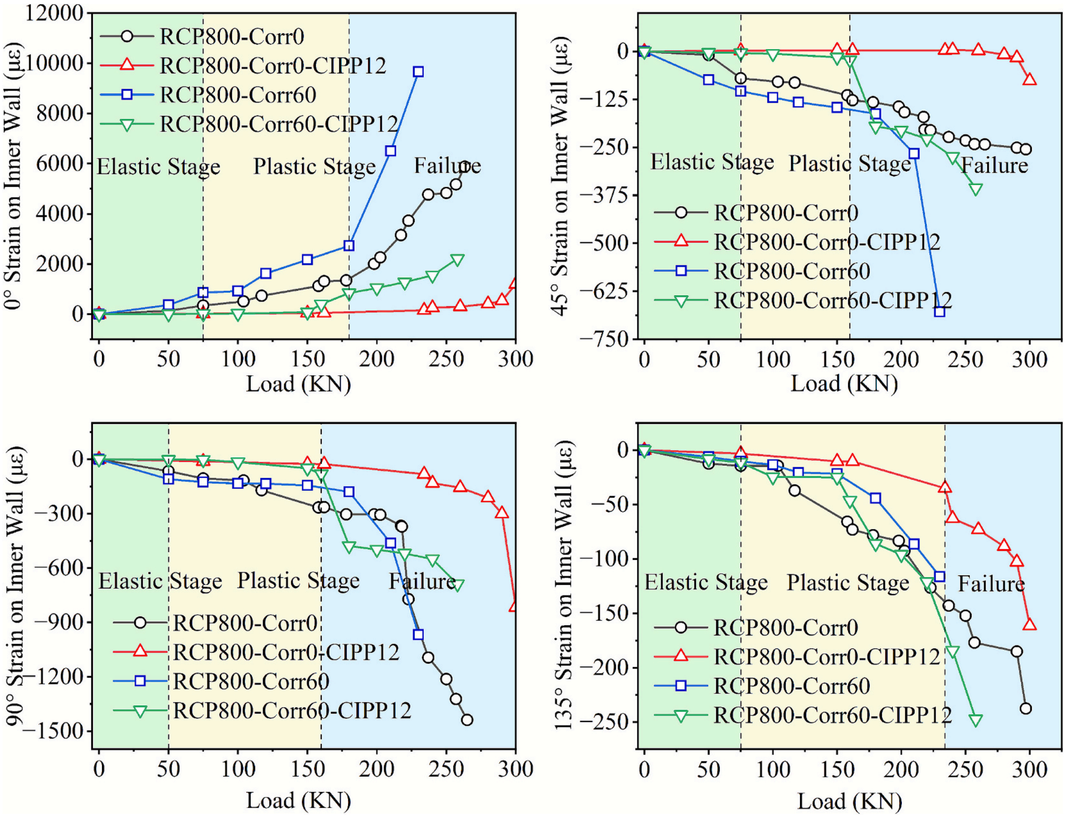

Fig. 12. Load–strain curves of DN800 single and composite pipe.

drops sharply, making them prone to circumferential cracking. The CIPP liner regulates the mechanical response through an asynchronous "circumferential peak reduction–gradient mitigation" mechanism: it first reduces high strain concentrations at 0°–180° (enhancing failure resistance) and then smooths the strain gradient from 90°–270° (enhancing crack resistance). Peaks exceeding 4000 με due to corrosion were reduced to about 1000 με, effectively eliminating abrupt transitions. This dual-stage redistribution—"peak reduction and gradient smoothing"—significantly decreases the likelihood of circumferential crack initiation.

3.4. Yield-to-Tensile strength ratio analysis

The yield-to-tensile strength ratio (σ_y/σ_u) is a key indicator of material ductility reserve, determining whether the CIPP lining can provide sufficient deformation capacity near the ultimate load to prevent sudden rupture. In this study, based on external pressure tests and load–strain curves, the circumferential membrane stress formulation together with the plane-section assumption was used to convert the cracking load P_y and ultimate load P_u into equivalent circumferential yield stress and ultimate stress. The results show that structural CIPP linings, owing to their relatively high yield-to-tensile strength ratio, develop a secondary yield plateau, increasing the yield-to-tensile strength ratio of reinforced concrete pipes from 0.66 to 0.71 to 0.78–0.80, thereby achieving a true brittle-to-ductile transition. For intact pipes, the increase in cracking load (25.68 %) exceeds that of ultimate load (10.77 %), reflecting the dominance of elastic-stage strengthening. In contrast, semi-structural repair exhibits a "pseudo-high" yield-to-tensile strength ratio (0.791) caused by stiffness–strength mismatch, which in reality corresponds to a faster decline in ultimate load and premature brittleness. Overall, changes in the yield-to-tensile strength ratio are strongly correlated with load increments and can serve as a primary control parameter for assessing the ductility of structural CIPP repair, with a recommended threshold of ≥ 0.75.

3.5. Crack distribution

Based on the strain distribution characteristics discussed above, the relationship between crack development and load-bearing capacity was further examined. Owing to the inherent brittleness of concrete, cracking can be triggered under complex service conditions, leading to various crack patterns and potential leakage or structural failure [32–38].

As shown in Fig. 14, transverse cracks first appeared on the outer wall along the springline and propagated bidirectionally through the wall thickness as well as circumferentially. Additional transverse cracks were observed at both the crown and the invert. At the crown, cracks were mainly distributed along the axial direction and nearby regions, whereas those at the invert were approximately

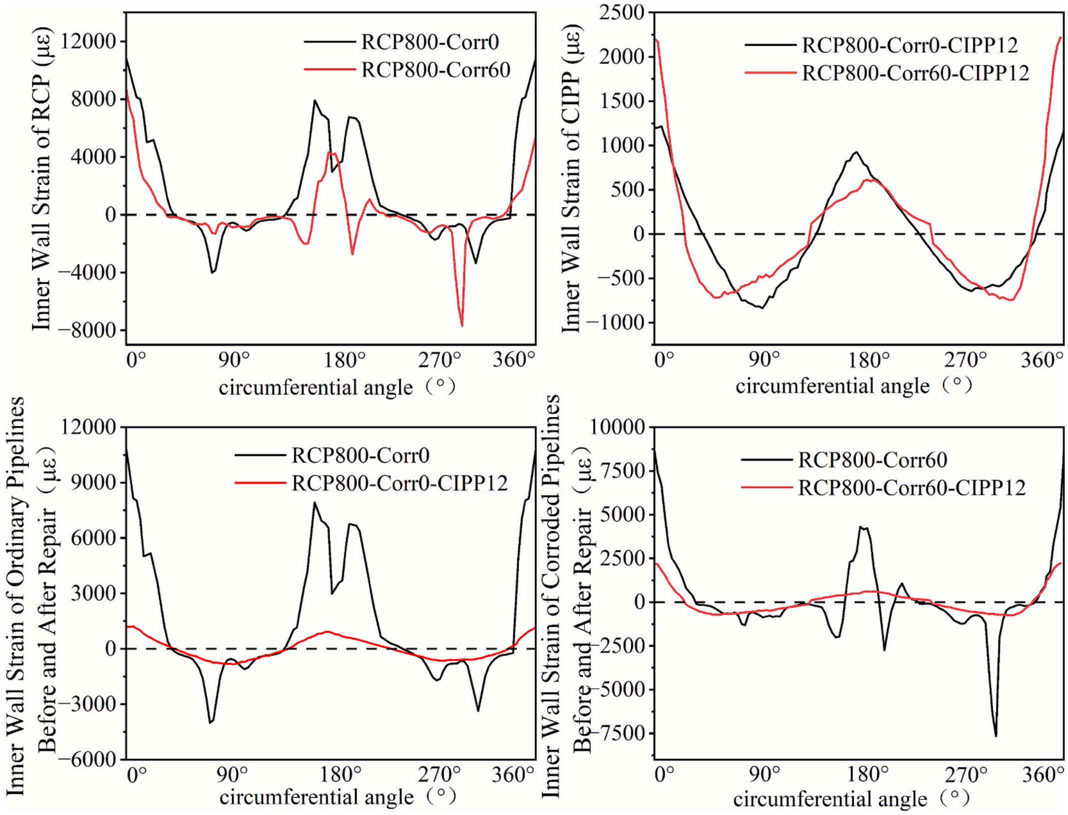

Fig. 13. Circumferential strain curves of single and composite pipes at different angles.

symmetric on both sides of the axis. Notably, the invert cracks concentrated in the midspan between the two rigid timber supports, while no comparable constraint existed at the crown. These observations indicate that differences in crack distribution between the crown and the invert are largely governed by the boundary conditions at the pipe base.

Table 5 summarizes the crack width measurements obtained during the experiments. For the plain RCPs, larger crack widths were associated with lower load-bearing capacity. After CIPP lining repair, the load-bearing capacity of pipes of the same diameter was significantly restored; however, continued crack propagation may diminish the effectiveness of this restoration.

The six data points shown represent averaged values derived from 18 full-scale specimens tested under six representative conditions. The exponential curve is fitted using all 18 raw measurements.

The relationship between crack width and ultimate load capacity (i.e., the residual load that the pipe can still sustain under TEBT at a given crack width) is presented in Fig. 15. As the crack width increases from 6 mm to 12 mm, the ultimate load decreases from approximately 266 kN to 210 kN and follows an exponential decay trend. Nonlinear least-squares fitting of all 18 test data points yields the following constitutive relationship:

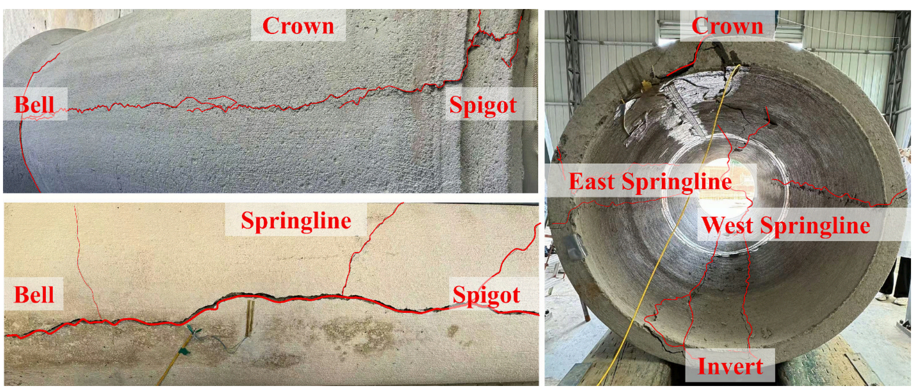

Fig. 14. Crack distribution on the inner and outer walls of the pipe.

Table 5
Crack width measurements.

Specimen	Nominal Pipe Diameter (mm)	Load-Bearing Capacity (kN)	Crack Width (mm)	Average Crack Width (mm)	Increment of Crack Width (%)
RCP 500-Corr0	500	210.33	12	11.0	/
		220.00	11		
		202.02	10		
RCP500-Corr0-CIPP5		189.22	10	8.0	−27.3 %
		160.63	8		
		174.73	6		
RCP800-Corr0	800	317.00	6	6.3	/
		237.00	7		
		241.00	6		
RCP800-Corr0-CIPP12		300.04	6	8.7	38.1 %
		280.05	10		
		300.56	10		
RCP800-Corr60		235.22	9	9.0	/
		210.00	9		
		230.00	9		
RCP800-Corr60-CIPP12		278.00	8	9.7	11.5 %
		261.02	11		
		258.38	10		

$$y = \frac{243.65}{1 + \exp(-0.39(x - 16.65))}, \quad R^2 = 0.96$$

The fitted curve exhibits excellent statistical performance, with $R^2 = 0.97769$, Adjusted $R^2 = 0.96281$, RSS = 15.32418, and RMSE = 1.6kN. These indicators show that, despite the modest sample size, the proposed exponential model captures the dependence of ultimate (residual) load capacity on crack width with high reliability.

3.6. Influence of CIPP rehabilitation on pipe failure modes

Fig. 16 summarizes the failure evolution observed in the experiments for both unreinforced and CIPP-rehabilitated pipes. The process generally followed four sequential stages: an initial intact condition; the initiation of tensile cracks at the crown or springline where circumferential tension was highest; the circumferential development and widening of these cracks as deformation increased; and finally, localized crushing or hinge-type failure in the critical regions. This schematic synthesizes the characteristic damage evolution repeatedly recorded in the tests and provides a clear overall reference for understanding the failure behavior of the pipes.

3.6.1. Failure modes of unreinforced concrete pipes

The test results indicate that, with increasing external pressure, stress progressively accumulated at crack tips, and once exceeding the tensile strength of concrete, abrupt fracture occurred along these cracks. As shown in Fig. 17, owing to the restraining and tensile effects of the steel cage, the RCP did not disintegrate into separate fragments; instead, cracks initiated at critical locations—such as the crown, invert, and springlines—and propagated longitudinally along the pipe, reflecting high structural stress.

With continued loading, crack widening progressively weakened the pipe, and brittle failure ultimately developed at these critical

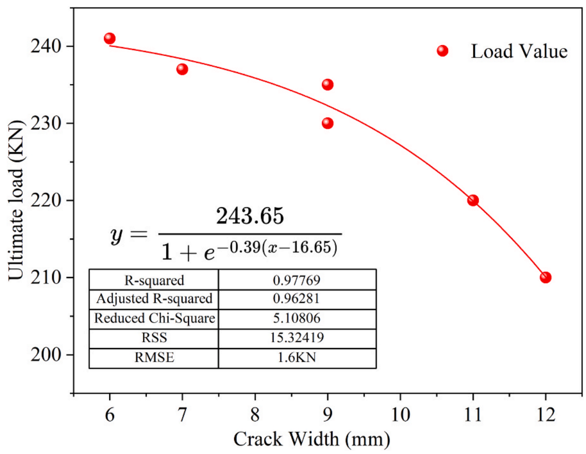

Fig. 15. Influence of Crack Width on Ultimate Load.

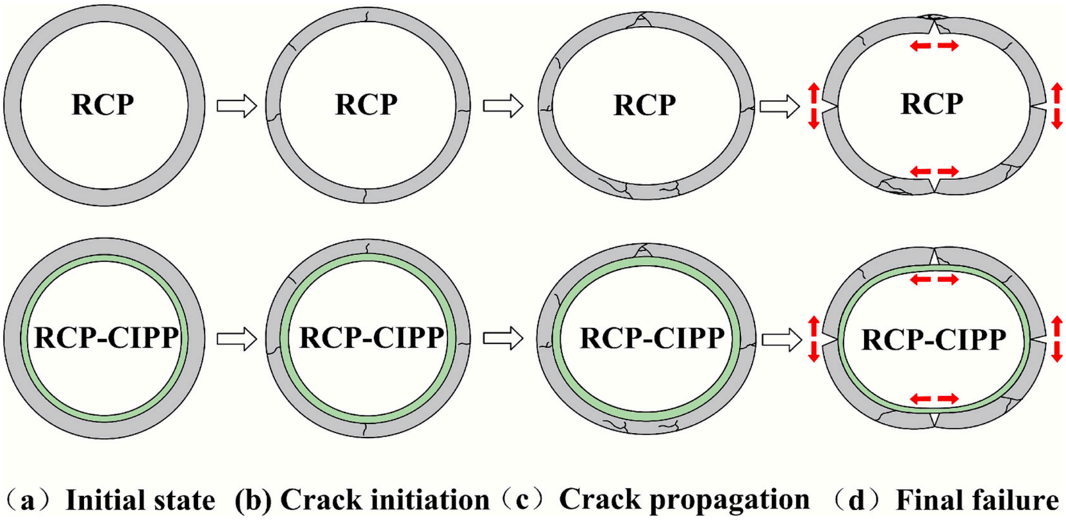

Fig. 16. Schematic illustration of crack evolution in unlined RCP and CIPP-rehabilitated RCP specimens: (a) Initial state, (b) Crack initiation, (c) Crack propagation, and (d) Final failure.

regions, accompanied by local concrete spalling and exposure of internal reinforcement. For pipes with corrosion defects, structural integrity and strength were further reduced, accelerating crack propagation and leading to premature structural collapse.

3.6.2. Failure mechanism of RCP-CIPP composite structure

The destructive testing results of the RCP–CIPP composite structure are shown in Figs. 18 and 19. The CIPP specimen exhibited a typical degradation pattern of flexible pipes under external loading, undergoing significant vertical deformation without initial damage until deformation reached approximately 20–30 % of the pipe diameter, at which point compressive failure occurred at the springlines. Compression of the fiber mesh led to local bulging of the surface resin layer.

The failure process of the RCP–CIPP composite can be summarized as follows: (1) crack initiation in critical zones of the host RCP; (2) debonding at the RCP–CIPP interface; (3) diagonal shear and tensile cracking of the RCP; (4) bulging, tearing, and delamination of the CIPP fiber–resin system due to structural deformation; and (5) compressive failure at the crown, invert, and springlines. Although the CIPP liner provides partial structural recovery, it remains susceptible to interfacial debonding and rupture in stress concentration regions.

3.7. Relevance to existing design standards

Existing CIPP design standards show limited applicability to rigid concrete pipes, particularly for semi-structural rehabilitation. Semi-structural design requires reliable assessment of the residual structural capacity of the host pipe and rational definition of liner–host pipe load sharing; however, current standards mainly focus on liner system performance and provide limited quantitative guidance on these aspects. Moreover, UV-cured CIPP liners generally behave as flexible pipes, whereas rigid concrete pipes are

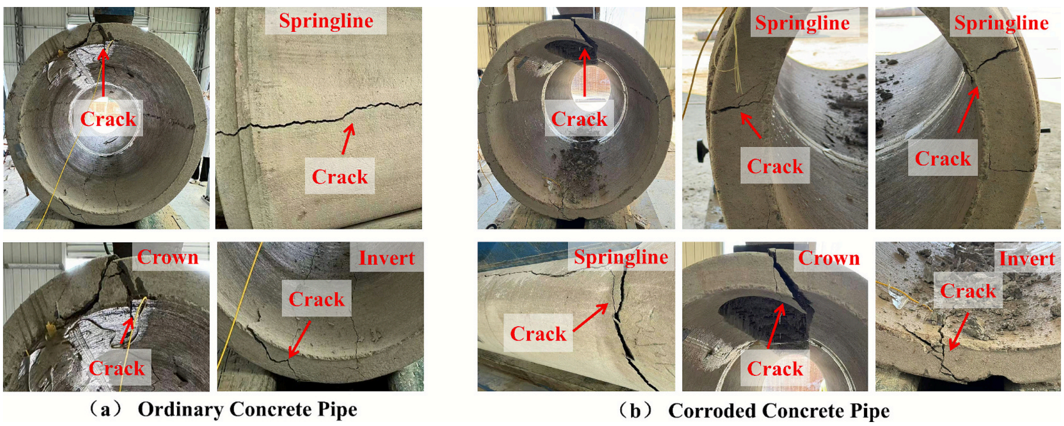

Fig. 17. Failure Modes of the Concrete Pipe Specimen:(a)Ordinary Concrete Pipe, and (b) Corroded Concrete Pipe.

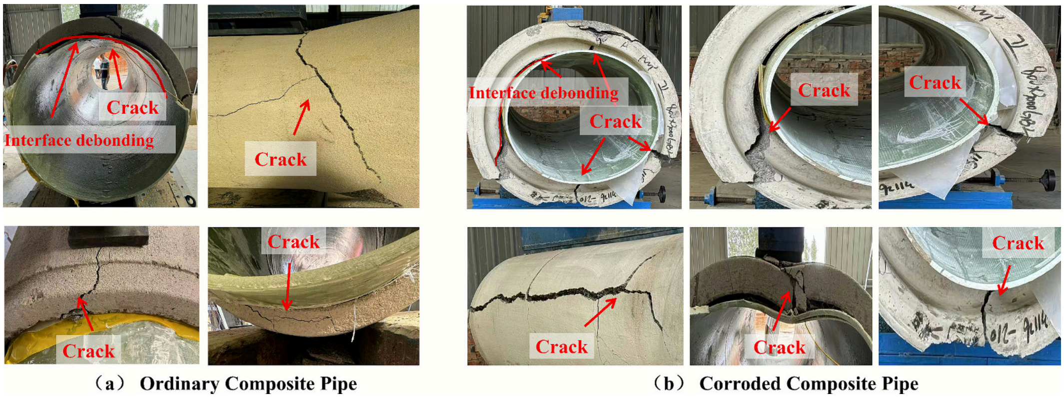

Fig. 18. Failure Modes of the RCP–CIPP Composite Specimen:(a)Ordinary Composite Pipe, and (b)Corroded Composite Pipe.

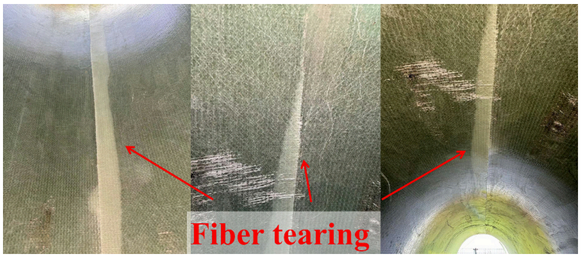

Fig. 19. Failure Cracking of the CIPP Liner.

governed by different external load–resistance mechanisms, making conventional design approaches based on ring stiffness or external pressure stability potentially inadequate for rigid–flexible composite systems.

In this context, ASTM F1216 relies on empirical thickness-based design and is commonly applied by treating the liner as an independent structural element, without explicitly addressing composite action or bending-dominated behavior under external loads. ISO 11296 emphasizes performance requirements and testing procedures but does not quantify stiffness interaction, stress redistribution, or neutral-axis migration in flexible–rigid composite pipes. In contrast, three-edge bearing tests in this study demonstrate that CIPP effectiveness under external loading is governed primarily by circumferential stiffness contribution and yield-to-ultimate strength characteristics rather than liner thickness alone. Structural liners exhibit clear stiffness superposition and neutral-axis migration, enhancing both load-carrying capacity and ductility, whereas semi-structural liners mainly delay crack initiation. These findings provide quantitative, mechanism-based criteria that complement existing standards for buried concrete pipes under external loads.

4. Conclusions

Based on the findings of this study, the following conclusions were drawn:

(1) The 12 mm structural CIPP liner increased the cracking and ultimate loads of reinforced concrete pipes by 10–26 % and improved ductility, whereas the 5 mm semi-structural liner provided limited or negative reinforcement due to insufficient circumferential stiffness.
(2) The experimental results align with the composite-beam model, confirming that circumferential stiffness superposition, neutral-axis shift, and compressive-gradient relaxation govern the enhanced bending resistance of CIPP-reinforced pipes.
(3) CIPP reinforcement reduced tensile and compressive strains and maintained stable composite action, with more significant benefits observed in corroded pipes.
(4) Cracks concentrated at the crown, invert, and sidewalls, and a strong negative exponential relationship was found between crack width and residual load capacity, offering a basis for rapid structural condition assessment.
(5) Under external loading, based on the experimental results for DN800 pipes, a 12 mm structural CIPP liner effectively mitigates stiffness degradation caused by crown corrosion and provides substantial improvements in both load-carrying capacity and ductility, making it suitable for structural rehabilitation. In contrast, tests on DN500 pipes with a 5 mm liner show only limited gains in strength and ductility, primarily associated with crack delay during the elastic stage, and such liners should therefore be restricted to non-structural rehabilitation. When corrosion depth exceeds 50–60 mm, the liner–host pipe composite action becomes increasingly significant, and structural CIPP liners should be prioritized to prevent premature brittle failure.

It should be noted that the findings of this study are based on short-term monotonic loading and do not account for long-term effects such as fatigue, creep, moisture ingress, temperature fluctuations, or chemical degradation. These time-dependent and environmental factors may influence stiffness interaction, liner–concrete bonding, and crack evolution during long-term service. Therefore, the present results should be interpreted within the context of short-term external loading. Future work incorporating cyclic loading, aging processes, and environmental conditioning is required to establish a more comprehensive understanding of the long-term performance of CIPP-rehabilitated concrete pipelines.

CRediT authorship contribution statement

Jing Liu: Writing – original draft, Resources, Methodology, Data curation. **Jingguo Cao:** Writing – review & editing, Investigation, Funding acquisition. **Chang Ma:** Validation, Investigation. **Wenlin Jing:** Validation, Investigation. **Kangfu Sun:** Writing – review & editing, Supervision, Conceptualization. **Tingting Yang:** Supervision, Project administration.

Declaration of competing interest

The authors declare that they have no known competing financial interests or personal relationships that could have appeared to influence the work reported in this paper.

Appendix A. Supplementary data

Supplementary data to this article can be found online at https://doi.org/10.1016/j.engfailanal.2026.110563.

Data availability

Data will be made available on request.

References

[1] R. Shahandeh, H. Showkati, Influence of ring-stiffeners on buckling behavior of pipelines under hydrostatic pressure, J. Constr. Steel Res. 121 (2016) 237–252, https://doi.org/10.1016/j.jcsr.2016.02.006.
[2] B. Bosseler, D. Homann, T. Brüggemann, I. Naismith, M. Rubinato, Quality assessment of CIPP lining in sewers: crucial knowledge acquired by IKT and research gaps identified in Germany, Tunn. Undergr. Space Technol. 143 (2024) 105425, https://doi.org/10.1016/j.tust.2023.105425.
[3] R. Serajiantehrani, M. Najafi, V. Kaushal, M. Malek Mohammadi, Life-cycle Assessment of Trenchless Cured-in-place Pipe (CIPP) Renewal Method in Large Diameter Stormwater Drainage Conduits, in: World Environmental and Water Resources Congress 2021, 2021, pp. 472–485.
[4] S. Das, A. Bayat, L. Gay, M. Salimi, J. Matthews, A comprehensive review of the challenges of cured-in-place pipe (CIPP) installations, J. Water Supply: Res. Technol.—AQUA 65 (8) (2016) 583–596, https://doi.org/10.1016/j.tust.2024.106357.
[5] Z. Zhong, S. Wang, M. Zhao, X. Du, L. Li, Performance of ductile iron push-on joints rehabilitated with CIPP liner under repetitive and seismic loadings, Soil Dyn. Earthq. Eng. 115 (2018) 776–786, https://doi.org/10.1016/j.soildyn.2018.09.031.
[6] Y. Xia, M. Shi, C. Zhang, C. Wang, X. Sang, R. Liu, H. Fang, Analysis of flexural failure mechanism of ultraviolet cured-in-place-pipe materials for buried pipelines rehabilitation based on curing temperature monitoring, Eng. Fail. Anal. 142 (2022) 106763, https://doi.org/10.1016/j.engfailanal.2022.106763.
[7] J. Jefrin, I. Subash, V. Manoj Kumar, CIPP: a trenchless rehabilitation overview, Int. J. Adv. Technol. Civil Eng. 1 (2) (2012) 31–36.
[8] T.C. Law, I.D. Moore. 18. Numerical Modeling of Tight Fitting Flexible Liner in Damaged Sewer under Earth Loads. Water and Energy Abstracts, 17(4) (2007) pp. 11-12. doi: 10.1016/j.tust.2006.11.006.
[9] T. Smith, N.A. Hoult, I.D. Moore, Role of grout strength and liners on the performance of slip-lined pipes, J. Pipeline Syst. Eng. Pract. 6 (4) (2015) 04015007, https://doi.org/10.1061/(ASCE)PS.
[10] E. Riahi, X. Yu, M. Najafi, V.F. Sever, D-load strength of concrete pipes with epoxy linings, J. Pipeline Syst. Eng. Pract. 10 (4) (2019) 04019030, https://doi.org/10.1061/(asce)ps.1949-1204.0000397.
[11] B. Simpson, N.A. Hoult, I.D. Moore, Rehabilitated reinforced concrete culvert performance under surface loading, Tunn. Undergr. Space Technol. 69 (2017) 52–63, https://doi.org/10.1016/j.tust.2017.06.007.
[12] H. Hu, F. Niu, T. Dou, H. Zhang, Rehabilitation effect evaluation of CFRP-Lined Prestressed Concrete Cylinder Pipe under combined Loads using Numerical simulation, Math. Probl. Eng. 2018 (1) (2018) 3268962, https://doi.org/10.1155/2018/3268962.
[13] X. Wang, C. Zeng, X. Yan, P. Zhang, Study on the bearing capacity of the polyethylene pipe–cured-in-place pipe liner composite structure under external pressure, Buildings 14 (7) (2024) 2253, https://doi.org/10.3390/buildings14072253.
[14] C. He, S. Dong, J. Li, J. Liao, Y. Wei, B. Ma, S. Huang, Experimental study on the structural performance of RCP rehabilitation by spraying method under preloading, Tunn. Undergr. Space Technol. 155 (2025) 106218, https://doi.org/10.1016/j.tust.2024.106218.
[15] K.J. Shou, B.C. Chen, Numerical analysis of the mechanical behaviors of pressurized underground pipelines rehabilitated by cured-in-place-pipe method, Tunn. Undergr. Space Technol. 71 (2018) 544–554, https://doi.org/10.1016/j.tust.2017.11.005.
[16] H. Fang, K. Yang, B. Li, H. He, B. Xue, Parameter Analysis of Wall Thickness of Cured-in-Place Pipe Linings for Semistructured Rehabilitation of Concrete Drainage Pipe, Math. Probl. Eng. 2020 (1) (2020) 5271027, https://doi.org/10.1155/2020/5271027.
[17] B. Li, H. Fang, K. Yang, X. Zhang, X. Du, N. Wang, X. Guo, Impact of erosion voids and internal corrosion on concrete pipes under traffic loads, Tunn. Undergr. Space Technol. 130 (2022) 104761, https://doi.org/10.1016/j.tust.2024.105651.
[18] J.M. Hsu, K.J. Shou, Numerical analysis of the mechanical behavior of separated joints in underground pipelines rehabilitated by cured-in-place pipes, Tunn. Undergr. Space Technol. 125 (2022) 104520, https://doi.org/10.1016/j.tust.2022.104520.
[19] Y. Takahashi, T. Deguchi, L. Li, K. Yamada, A study of the bedding effects of the deteriorated existing pipe on the flexible rehabilitated pipe and its mechanism, J. Jpn Sew Works Assoc. 39 (471) (2002) 103–115.
[20] J. Gumbel, A. Spasojevic, R. Mair. Centrifuge modelling of soil load transfer to flexible sewer liners. in: New Pipeline Technologies, Security, and Safety, (2003) (pp. 352-362).

[21] K. Yang, H. Fang, J. Bu, X. Zhang, B. Li, X. Du, Z. Zhang, Full-scale experimental investigation of the mechanical characteristics of corroded buried concrete pipes after cured-in-place-pipe rehabilitation, Tunn. Undergr. Space Technol. 117 (2021) 104153, https://doi.org/10.1016/j.tust.2021.104153.
[22] H. Fang, J. Sun, B. Li, X. Du, N. Wang, D. Di, K. Zhai, Longitudinal and circumferential bending moment responses of dislocated concrete pipes rehabilitated with CIPP liners under traffic loads, Tunn. Undergr. Space Technol. 155 (2025) 106222, https://doi.org/10.1016/j.tust.2024.106222.
[23] K. Yang, J. Zhang, H. Fang, S. Ma, L. Shi, B. Li, K. Zhai, Mechanical performances of the pipe-liner structure under void conditions, Tunn. Undergr. Space Technol. 159 (2025) 106484, https://doi.org/10.1016/j.tust.2025.106484.
[24] X.F. Yan, Y.Y. Jiao, C. Zeng, S.T. Ariaratnam, Z.Y. Zhao, Residual load capacity of longitudinally-cracked reinforced-concrete pipe and its recovery by CIPP versus spray-mortar liners, Tunn. Undergr. Space Technol. 168 (2026) 107126, https://doi.org/10.1016/j.tust.2025.107126.
[25] V. Kaushal, M. Najafi, Investigation of microbiologically influenced corrosion of concrete in sanitary sewer pipes and manholes: field surveys and laboratory assessment, Adv. Environ. Eng. Res. 03 (02) (2022) 1–16, https://doi.org/10.21926/aeer.2202027.
[26] N. Stanić, J. Langeveld, T. Salet, F. Clemens, Relating the structural strength of concrete sewer pipes and material properties retrieved from core samples, Struct. Infrastruct. Eng. 13 (5) (2016) 637–651, https://doi.org/10.1080/15732479.2016.1187631.
[27] E. Kuliczkowska, A. Parka, The structural integrity of corroded concrete sewers, Eng. Fail. Anal. 104 (2019) 409–421, https://doi.org/10.1016/j.engfailanal.2019.06.012.
[28] P. Zhang, C. Gong, Q. Wu, C. Zeng, Experimental study on the bearing capacity of reinforced concrete pipes with corrosion-thinning defects repaired by UHP-ECC mortar spraying, Appl. Sci. 13 (13) (2023), https://doi.org/10.3390/app13137800.
[29] H. Wang, B. Li, H. Fang, X. Du, N. Wang, Q. Zang, D. Di, Interface bonding characteristics of the Cured-in-Place Pipe lined steel plates and parameter sensitivity analysis, Structures 69 (2024), https://doi.org/10.1016/j.istruc.2024.107574.
[30] X. Wang, Y. Zhao, S.T. Ariaratnam, X. Yan, Study on the impact of ovality defect on structural stability of CIPP liner of drainage pipeline, Tunn. Undergr. Space Technol. 140 (2023) 105338, https://doi.org/10.1016/j.tust.2023.105338.
[31] G. Ranzi, G. Leoni, R. Zandonini, State of the art on the time-dependent behaviour of composite steel–concrete structures, J. Constr. Steel Res. 80 (2013) 252–263, https://doi.org/10.1016/j.jcsr.2012.08.005.
[32] A. Akram, Z. Mustaffa, T.M.B. Albarody, Burst capacity of pipe under corrosion defects and repaired with thermosetting liner steel and composite structures, Int. J. 35 (2) (2020) 171–186, https://doi.org/10.12989/scs.2020.35.2.171.
[33] A. Selvakumar, A.N. Tafuri, Rehabilitation of aging water infrastructure systems: key challenges and issues, J. Infrastruct. Syst. 18 (3) (2012) 202–209, https://doi.org/10.1061/(asce)is.1943-555x.0000091.
[34] J.D. Wise, A.J. Wagner. The Modified use of the Rehabilitation of Water Mains Manual, AWWA M28 and ASTM , to Design Large Diameter pressure Pipes using FRP Systems. In Pipelines (2015) pp. 374 385.
[35] Y. Zhao, Y. Chen, X. Yan, P. Ma, H. Zhang, B. Ma, S. Huang, Impact of bedding layers to soil-pipe-liner structure under static and traffic loads with EPR technology, Tunn. Undergr. Space Technol. 146 (2024) 105651, https://doi.org/10.1016/j.tust.2024.105651.
[36] C. Garcia, D.M. Abraham, S. Gokhale, T. Iseley, Rehabilitation alternatives for concrete and brick sewers, Pract. Period. Struct. Des. Constr. 7 (4) (2002) 164–173, 10.1061/.
[37] H. Zhu, Y. Hu, Q. Li, R. Ma, Restrained cracking failure behavior of concrete due to temperature and shrinkage, Constr. Build. Mater. 244 (2020) 118318, https://doi.org/10.1016/j.conbuildmat.2020.118318.
[38] A.A. Jain. Evaluation of trenchless renewal methods for potable water distribution pipes (Doctoral dissertation, University of Texas at Arlington) (2010).